

Cite this: *J. Mater. Chem.*, 2012, **22**, 6869

www.rsc.org/materials

PAPER

Blue light-emitting and hole-transporting materials based on 9,9-bis(4-diphenylaminophenyl)fluorenes for efficient electroluminescent devices†

A-monrat Thangthong, Narid Prachumrak, Ruangchai Tarsang, Tinnagon Keawin, Siriporn Jungsuttiwong, Taweesak Sudyoasuk and Vinich Promarak*

Received 27th October 2011, Accepted 22nd January 2012

DOI: 10.1039/c2jm15480c

New bifunctional materials namely **BTTF**, **TPTF** and **BPTF** having 9,9-bis(4-diphenylaminophenyl)fluorene as a molecular platform were synthesized and characterized. These molecules showed strong blue emission in both solution and solid state with a solution fluorescence quantum efficiency of up to 74% and were thermally stable amorphous materials with glass transition temperature well above 170 °C. The abilities of these materials as blue light-emitting materials for blue OLEDs and hole-transporting materials for green OLEDs in terms of device performance and thermal property were superior to a commonly used *N,N'*-diphenyl-*N,N'*-bis(1-naphthyl)-(1,1'-biphenyl)-4,4'-diamine (NPB). Efficient non-doped blue and Alq3-based green OLEDs with maximum luminance efficiencies and *CIE* coordinates of 2.06 cd A⁻¹ and (0.15, 0.13), and 4.94 cd A⁻¹ and (0.29, 0.52) were achieved, respectively, with **BPTF** having two pyrene substituents as the emitting layer and the hole-transporting layer, respectively.

Introduction

Organic light-emitting diodes (OLEDs) have attracted a great deal of attention due to their applications, such as in full-color or large-area flat panel displays, backlights, and general illumination.¹ In the past decade, we have seen great progress in both materials development and device fabrication techniques.² One area of continuing research is the pursuit of a stable-blue emitting material. Poly(*p*-phenylene) (PPP)³ and related polymers, such as ladder-type PPP and polyfluorenes (PFs), have received strong interest in recent years.⁴ Although PFs in particular have been used to make efficient blue light-emitting devices,⁵ they still have a number of deficiencies as potential candidates for blue OLEDs including low colour purity due to side emission from the aggregates and defect sites, and requiring the use of hole-transporting layers to obtain a balance in charge carriers.⁶ The hole-injection ability of these PFs has been successfully improved by many approaches such as blending with hole-transporting triarylamine,⁷ end-capping the polymer chain with triarylamine,⁸ copolymerization with triarylamine-containing monomers⁹ and substitutions at the C-9 position of the fluorene block

with triarylamine.¹⁰ The latter approach was proven to be more effective and less complex synthesis is required. For example, 9,9-bis(4-diphenylaminophenyl)fluorene (9,9-bis(triphenylamine)fluorene) has been successfully used as a building block for the synthesis of many blue emitting PFs and copolymers with improving hole-injection and suppressing aggregation.¹¹ It has been shown that the formation of molecular fluorenes or oligofluorenes efficiently improved the colour purity of these polymers.¹² Hence, using this fluorene building block to construct new molecular materials might be a simple solution to develop efficient pure blue emitters.

Owing to its high photoluminescence efficiency in the blue region, high carrier mobility, and improved hole-injection ability than other blue chromophores such as oligofluorenes, PFs or PPP, pyrene has been used as a building block to form many emissive materials.¹³ Recently, many kinds of pyrene-functionalized materials have been synthesized and considered for several applications,¹⁴ and some of them are proven to be promising blue emitters for OLEDs.¹⁵ Pyrene-based molecules as bifunctional materials, blue emitters and hole-transporters remain rare and largely unexplored in OLEDs.¹⁶ Therefore, we herein implemented all required aspects in the synthesized molecules (Fig. 1). The use of 9,9-bis(4-diphenylaminophenyl)fluorene as a molecular framework offers a perfect bulky molecule with high thermal stability and an improved hole injection and transport ability from the substituted triphenylamine units. Incorporation of a pyrene unit into the cruciform of this platform is an effective way to control the π - π stacking interactions and to maintain the high blue emissive ability of pyrene in the solid state, which

Center for Organic Electronic and Alternative Energy, Department of Chemistry and Center for Innovation in Chemistry, Faculty of Science, Ubon Ratchathani University, Warinchumrap, Ubon Ratchathani, 34190, Thailand. E-mail: pvinich@ubu.ac.th; pvinich@gmail.com; Fax: +66 4528 8379; Tel: +66 4535 3400 ext. 4510

† Electronic supplementary information (ESI) available: Synthesis of **2**, CV curves, energy diagrams and EL spectra of the devices, and ¹H-, ¹³C-NMR and mass spectra. See DOI: 10.1039/c2jm15480c.

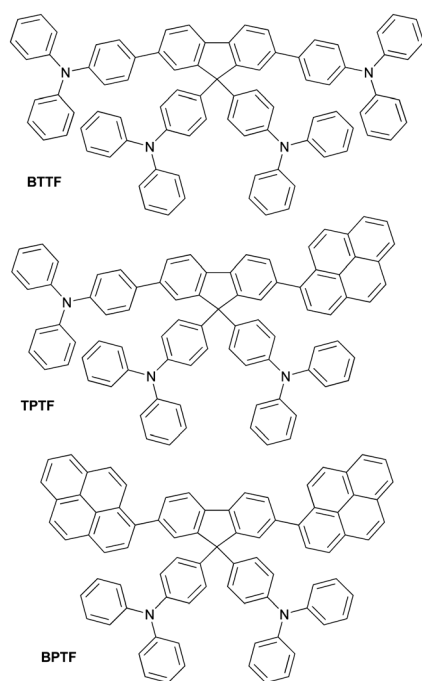


Fig. 1 Molecular structures of BTTF, TPTF and BPTF.

significantly impact the emission behaviour of devices. The high steric hindrance in the molecule also offers good solubility and thereby thermally stable amorphous thin film could be deposited by a cheap solution process. Fluorene also has a number of advantages, including its capability to emit in the blue part of the visible spectrum, chemical and photochemical stability.^{4,5,12} Accordingly, this would result in new bifunctional materials with combined blue-emitting and hole-transporting properties. An investigation of their physical and photophysical properties, and blue OLED fabrication and characterization is also reported.

Experimental section

General procedure

¹H and ¹³C nuclear magnetic resonance (NMR) spectra were recorded on a Bruker AVANCE 300 MHz spectrometer with tetramethylsilane as the internal reference using CDCl₃ as the solvent in all cases. Infrared (IR) spectra were measured on a PerkinElmer FTIR spectroscopy spectrum RXI spectrometer as potassium bromide (KBr) disc. Ultraviolet-visible (UV-Vis) spectra were recorded for a dilute solution in dichloromethane on a PerkinElmer UV Lambda 25 spectrometer. Photoluminescence spectra and the fluorescence quantum yields (Φ_F) were recorded with a PerkinElmer LS 50B Luminescence Spectrometer for a dilute solution in dichloromethane and a thin film obtained by thermal evaporation. A quinine sulfate solution in 0.01 M H₂SO₄ ($\Phi_F = 0.54$) was used as the reference standard.¹⁷ Differential scanning calorimetry (DSC) analysis and thermogravimetry analysis (TGA) were performed on a METTLER DSC823e thermal analyzer and a Rigaku TG-DTA 8120 thermal analyzer, respectively, with a heating rate of 10 °C min⁻¹ under nitrogen atmosphere. Cyclic voltammetry (CV) measurements were carried out on an Autolab potentiostat PGSTAT 12

with a three electrode system (platinum counter electrode, glassy carbon working electrode and Ag/Ag⁺ reference electrode) at a scan rate of 50 mV s⁻¹ in the presence of tetrabutyl ammonium hexafluorophosphate (*n*-Bu₄NPF₆) as a supporting electrolyte in dichloromethane under argon atmosphere. Melting points were measured using an Electrothermal IA 9100 series of digital melting point instruments and are uncorrected. High resolution mass spectrometry (HRMS) analysis was performed on Bruker micrOTOF (Q-ToF II) mass spectrometer. Elemental analysis was performed on a PerkinElmer 2400 Series II CHNS/O Elemental Analyzer at Chulalongkorn University.

Synthesis

2,7,9,9-Tetrakis(4-diphenylaminophenyl)fluorene (BTTF). A mixture of **2** (1.00 g, 0.55 mmol), triphenylamine-4-boronic acid (0.39 g, 1.35 mmol), Pd(PPh₃)₄ (21 mg, 0.13 mmol) and an aqueous Na₂CO₃ solution (2 M, 10 ml) in THF (15 ml) was degassed with N₂ for 5 min. The mixture was heated at reflux under N₂ atmosphere for 20 h. After the mixture was cooled to room temperature water (50 ml) was added. The mixture was extracted with CH₂Cl₂ (50 ml × 2). The combined organic phase was washed with water (50 ml) and brine solution (50 ml), dried over anhydrous Na₂SO₄, filtered, and the solvents were removed to dryness. Purification by column chromatography using silica gel eluting with a mixture of CH₂Cl₂ and hexane followed by recrystallisation in a mixture of CH₂Cl₂ and methanol afforded white solids (1.09 g, 78%); mp 200–201 °C; ¹H NMR (300 MHz, CDCl₃) δ 6.92–7.09 (20H, m), 7.16–7.31 (32H, m), 7.47 (4H, d, $J = 8.40$ Hz), 7.50 (2H, d, $J = 9.01$ Hz), 7.61 (2H, s), 7.8 (2H, d, $J = 7.8$ Hz); ¹³C NMR (75 MHz, CDCl₃) δ 64.68, 120.35, 122.77, 122.99, 123.09, 123.81, 124.45, 126.15, 127.79, 129.00, 129.17, 129.29, 135.24, 138.62, 139.62, 140.01, 146.27, 147.19, 147.65, 147.71, 152.52; IR (KBr disc) 3415, 3031, 1600, 1505, 1250, 1177, 813; found: C, 89.71; H, 5.34; N, 5.65%; HRMS (m/z) M⁺, 1139.5376. C₈₅H₆₂N₄ requires C, 89.60; H, 5.48; N, 4.92%; M⁺, 1138.4977.

2,7-Bis(pyrene-1-yl)-9,9-bis(4-diphenylaminophenyl)fluorene (BPTF). BPTF was synthesized in the same manner as BTTF from **2** and pyrene-1-boronic acid, and obtained as yellow solids (0.56 g, 68%); mp > 250 °C; ¹H NMR (300 MHz, CDCl₃) δ 6.98 ppm (8H, t, $J = 9.01$ Hz), 7.07 (8H, d, $J = 7.69$ Hz), 7.15–7.29 (20H, m), 7.51 (2H, d, $J = 8.18$ Hz), 7.67 (2H, d, $J = 7.85$ Hz), 7.77 (2H, s), 7.89–8.00 (2H, m), 8.03–8.06 (2H, m), 8.10 (4H, t, $J = 7.23$ Hz), 8.22 (2H, t, $J = 8.10$ Hz); ¹³C NMR (75 MHz, CDCl₃) δ 50.50, 120.44, 122.73, 123.45, 124.30, 124.72, 124.80, 124.94, 125.12, 125.18, 125.26, 126.07, 127.44, 127.50, 127.69, 128.48, 128.83, 129.05, 129.21, 130.05, 130.64, 130.97, 131.53, 137.77, 138.96, 140.51, 146.39, 147.73; IR (KBr disc) 3415, 3031, 1589, 1510, 1260, 813; found: C, 92.32; H, 5.28; N, 2.59%; HRMS (m/z) M⁺, 1052.4506. C₈₁H₅₂N₂ requires C, 92.36; H, 4.98; N, 2.66%; M⁺, 1052.4130.

7-Bromo-2,9,9-tris(4-diphenylaminophenyl)fluorene (3). **3** was synthesized in the same manner as BTTF from **2** and triphenylamine-4-boronic acid, and obtained as white solids (1.02 g, 72%); mp 167–170 °C; ¹H NMR (300 MHz, CDCl₃) δ 6.93 ppm (4H, d, $J = 9.01$), 7.00 (5H, t, $J = 8.10$), 7.15–7.07 (19H, m), 7.31–7.21

(12H, m), 7.46 (2H, d, $J = 7.840$), 7.51 (1H, s), 7.58 (1H, s), 7.62 (2H, d, $J = 5.10$), 7.64 (1H, s), 7.77 (1H, d, $J = 7.8$ Hz); ^{13}C NMR (75 MHz, CDCl_3) δ 64.66, 120.45, 120.45, 121.16, 121.42, 122.92, 123.07, 123.70, 124.40, 124.56, 126.25, 127.77, 128.84, 129.22, 129.30, 129.37, 130.66, 137.68, 138.65, 138.87, 140.58, 146.48, 147.60, 152.09, 153.88; IR (KBr disc) 3415, 3030, 1600, 1520, 1256, 1170, 813; found: C, 82.44; H, 5.31; N, 4.37%; HRMS (m/z) M^+ , 973.3099. $\text{C}_{67}\text{H}_{48}\text{BrN}_3$ requires C, 82.53; H, 4.96; N, 4.31%; M^+ , 973.3032.

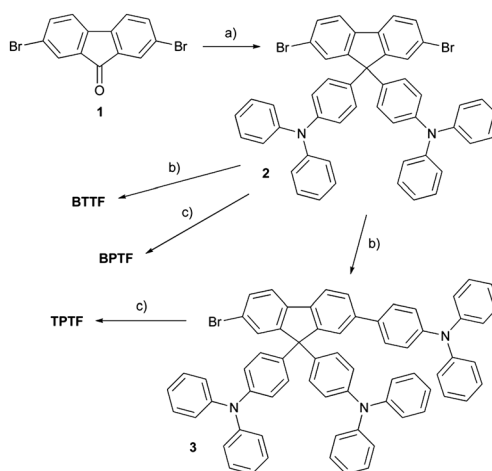
7-(Pyren-1-yl)-2,9,9-tris(4-diphenylaminophenyl)fluorene (TP-TF). TP-TF was synthesized in the same manner as BTTF from **3** and pyrene-1-boric acid, and obtained as light yellow solids (0.48 g, 75%); mp 189–199 °C; ^1H NMR (300 MHz, CDCl_3) δ 6.99 ppm (8H, t, $J = 6.90$ Hz), 7.12 (10H, d, $J = 7.00$ Hz), 7.29 (24H, m), 7.48 (2H, d, $J = 12$ Hz), 7.62 (3H, t, $J = 12$ Hz), 7.68 (1H, s), 7.87–7.95 (3H, m), 7.98–8.03 (2H, m), 8.08 (4H, t, $J = 12$ Hz); ^{13}C NMR (75 MHz, CDCl_3) δ 64.74, 120.24, 120.63, 122.76, 123.30, 124.38, 124.70, 124.77, 124.93, 125.09, 125.15, 125.26, 126.05, 127.45, 127.67, 128.45, 128.70, 129.02, 129.19, 129.91, 130.59, 130.95, 131.51, 137.79, 138.89, 139.68, 140.25, 146.30, 147.69, 152.38; IR (KBr disc) 3415, 3031, 1602, 1504, 1260, 813; found: C, 91.13; H, 5.36; N, 3.89%; HRMS (m/z) M^+ , 1096.4537. $\text{C}_{83}\text{H}_{59}\text{N}_3$ requires C, 90.93; H, 5.24; N, 3.83%; M^+ , 1097.4709.

Quantum calculation

The ground state geometries of all molecules were fully optimized using density functional theory (DFT) at the B3LYP/6-31G (d,p) level, as implemented in Gaussian 03.¹⁸ TDDFT/B3LYP calculation of lowest excitation energies was performed at the optimized geometries of the ground states.

Fabrication and characterisation of OLEDs

OLED devices using BTTF, TP-TF and BPTF as EML with a configuration of ITO/PEDOT:PSS/EML(50 nm)/BCP(40 nm)/LiF(0.5 nm):Al(150 nm) and double-layer green OLED devices using BTTF, TP-TF, BPTF and NPB as HTL with a configuration of ITO/PEDOT:PSS/HTL(40 nm)/Alq3(50 nm)/LiF(0.5 nm):Al(150 nm) were fabricated and characterized as followed. The patterned indium tin oxide (ITO) glass substrate with a sheet resistance $14 \Omega \square^{-1}$ (purchased from Kintec Company) was thoroughly cleaned by successive ultrasonic treatment in detergent, deionised water, isopropanol, and acetone, and then dried at 60 °C in a vacuum oven. A 50 nm thick PEDOT:PSS hole injection layer was spin-coated on top of ITO from a 0.75 wt% dispersion in water at a spin speed of 3000 rpm for 20 s and dried at 200 °C for 15 min under vacuum. Thin films of each organic EML or HTL were deposited on top of the PEDOT:PSS layer by evaporation from resistively heated alumina crucibles at the evaporation rate of 0.5–1.0 nm s^{-1} in vacuum evaporator deposition (ES280, ANS Technology) under a base pressure of $\sim 10^{-5}$ mbar. The film thickness was monitored and recorded by a quartz oscillator thickness meter (TM-350, MAXTEK). A 40 nm thick hole-blocking layer of BCP or a 50 nm thick green-emitting layer of Alq3 was then deposited on the organic EML or HTL, respectively, without breaking the vacuum chamber. The chamber was vented with dry air to load



Scheme 1 Synthesis of BTTF, TPTF and BPTF: (a) triphenylamine, MeSO_3H , 190 °C; (b) pyrene-1-boric acid; (c) triphenylamine-4-boric acid, $\text{Pd}(\text{PPh}_3)_4$, 2 M Na_2CO_3 , THF, reflux.

the cathode materials and pumped back; a 0.5 nm thick LiF and a 150 nm thick aluminium layers were subsequently deposited through a shadow mask on the top of EML/HTL film without breaking vacuum to form an active diode area of 4 mm^2 . The measurement of the device efficiency was performed according to M.E. Thomson's protocol and the device external quantum efficiencies were calculated using a procedure reported previously.¹⁹ Current density–voltage–luminescence (J – V – L) characteristics were measured simultaneously by the use of a Keithley 2400 source meter and a Newport 1835C power meter equipped with a Newport 818-UV/CM calibrated silicon photodiode. The EL spectra were acquired by an Ocean Optics USB4000 multi-channel spectrometer. All the measurements were performed under ambient atmosphere at room temperature.

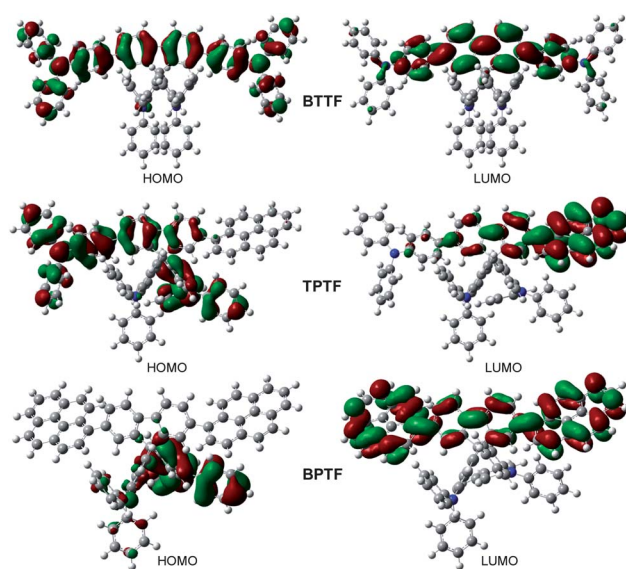


Fig. 2 The HOMO (right) and LUMO (left) orbitals of BTTF, TPTF and BPTF.

Results and discussion

Synthesis

The target molecules were synthesized as outlined in Scheme 1. Firstly, an intermediate **2** was synthesized *via* a tandem protocol of readily obtained 2,7-difluorenone (**1**) with an excess of triphenylamine catalysed by methanesulfonic acid at 190 °C. Coupling of **2** with either pyrene-1-boronic acid or triphenylamine-4-boronic acid by the Suzuki cross-coupling reaction catalysed by Pd(PPh₃)₄ afforded **BPTF** and **BTTF** in good yields as yellow and white solids, respectively. Under the same Pd-catalysed coupling conditions, a stepwise coupling of **2** with triphenylamine-4-boronic acid followed by 1-pyreneboronic acid gave **TPTF** as a light yellow solid in 54% yield over two steps. Their chemical structures were characterized unambiguously with ¹H-NMR, ¹³C-NMR spectroscopy and mass spectrometry. These materials showed good solubility in organic solvents, opening the door to solution processing techniques.

Quantum calculation and optical properties

To understand the electronic properties and the geometries of the synthesized molecules, quantum chemical calculations were performed using the TDDFT/B3LYP/6-31G (d,p) method.¹⁸ The optimized structures of these compounds revealed that both triphenylamine moieties at the C-9 position of the fluorene ring generated high steric hindrance, resulting in a bulky molecular structure and thereby preventing a closed π - π stacking interaction of the molecule. The molecules (**TPTF** and **BTTF**) became more steric when the C-2 or -7 positions of the fluorene ring being attached by extra triphenylamine units. In the highest occupied molecular orbitals (HOMO) of **BTTF** and **TPTF**, π -electrons delocalized over the π -conjugated 2-(4-diphenylaminophenyl)fluorene backbone and also located on triphenylamine pendant groups, while in the HOMO orbital of **BPTF**, π -electrons localized only on the triphenylamine (Fig. 2). This suggested that there is no π -electron interaction between the fluorene and pyrene moieties. In the lowest unoccupied molecular orbitals (LUMO) of all compounds, the excited electrons delocalized over the quinoid-like pyrene-fluorene plane, created in the case of **TPTF** a donor-acceptor molecule with triphenylamine acting as the donor and pyrene acting as the acceptor. The HOMO-LUMO energy gaps (E_g cal.) were calculated and are presented in Table 1. These calculated values slightly deviated from those

obtained from the experimental results (~0.03 to 0.11 eV). There are factors responsible for the errors because the orbital energy difference between HOMO and LUMO is still an approximate estimation of the transition energy since the transition energy also contains significant contributions from some two-electron integrals. The real situation is that an accurate description of the lowest singlet excited state requires a linear combination of a number of excited configurations.

The optical properties of **BTTF**, **TPTF** and **BPTF** were investigated in dilute CH₂Cl₂ solution and thin film obtained by thermal evaporation on a quartz substrate. The pertinent data are presented in Fig. 3a and summarized in Table 1. Their solution absorption spectra showed two absorption bands: a strong absorption band at 303 nm corresponding to the π - π^* local electron transition of the pendant triphenylamine moieties and a less intense absorption band at a longer wavelength (350–400 nm) assigned to the π - π^* electron transition of the π -conjugated backbone. In solid state, similar absorption features with a slight red shift compared to their corresponding solution spectra were observed. These materials exhibited a strong blue fluorescence in both solution and solid state. The fluorescence quantum yields (Φ_F) of **BTTF**, **TPTF** and **BPTF** measured in dilute solution using quinine sulfate solution in 0.01 M H₂SO₄ ($\Phi_F = 0.54$) as a standard were 0.43, 0.64 and 0.74, respectively. The results indicated that the direct attachment of the pyrene ring to the molecule boosted the Φ_F of these materials. Their solution photoluminescence (PL) spectra showed a featureless emission peak in the blue region (430–470 nm). The PL spectrum of **TPTF** red-shifted by 28 nm with respect to those of **BTTF** and **BPTF**, resulting from its donor-acceptor character as indicated by quantum calculation. These materials showed small Stokes shifts (66–89 nm) suggesting less energy loss during the relaxation process and thereby ensuing efficient fluorescence. The thin film PL emission spectra of **BTTF** and **BPTF** were similar to their solution PL spectra, hence indicating no or less if any solid state packing occurred in this case due to their bulky molecular structures.

Thermal and electrochemical properties

For OLED applications, thermal stability of organic materials is crucial for device stability and lifetime. The thermal instability or low glass transition temperature (T_g) of the amorphous organic layer may result in the degradation of organic devices due to

Table 1 Physical data of the synthesized molecules

Comp.	Solution ^a /nm			Thin film ^c /nm			Φ_F^d	$(T_g/T_{5d})^e/^\circ\text{C}$	$E_{1/2} (E_{\text{onset}})^f/\text{V}$	E_g^g/eV	$E_g \text{ cal}^h/\text{eV}$	HOMO/LUMO ⁱ /eV
	λ_{abs}	λ_{em}	Stokes shift ^b	λ_{abs}	λ_{em}							
BTTF	303, 363	437	71	310, 375	436	0.43	171/390	0.96 (0.85)	3.06	3.11	–5.29/–2.23	
TPTF	303, 373	462	89	310, 380	447	0.64	174/405	0.98, 1.27 (0.87)	3.01	3.04	–5.31/–2.30	
BPTF	303, 369	436	66	310, 375	441	0.74	179/472	0.97, 1.13 (0.87)	3.02	3.13	–5.31/–2.28	

^a Measured in CH₂Cl₂ solution. ^b Stokes shift calculated from the difference between λ_{max} of the absorption and emission spectra. ^c Measured on the thermal evaporated film on a quartz substrate. ^d Determined in CH₂Cl₂ solutions ($A < 0.1$) at room temperature using quinine sulfate solution in 0.01 M H₂SO₄ ($\Phi_F = 0.54$) as a standard. ^e Obtained from DSC (2nd heating scan) and TGA at a heating rate of 10 °C min⁻¹. ^f Measured by CV (Pt counter, glassy carbon working and SCE reference electrodes) in CH₂Cl₂ containing *n*-Bu₄NPF₆ as a supporting electrolyte. ^g Estimated from the optical absorption edge. ^h Obtained from the quantum chemical calculation using TDDFT/B3LYP/6-31G (d,p). ⁱ Calculated by HOMO = $-(4.44 + E_{\text{onset}})$, and LUMO = HOMO – E_g , where E_{onset} is the onset potential of the oxidation peak.

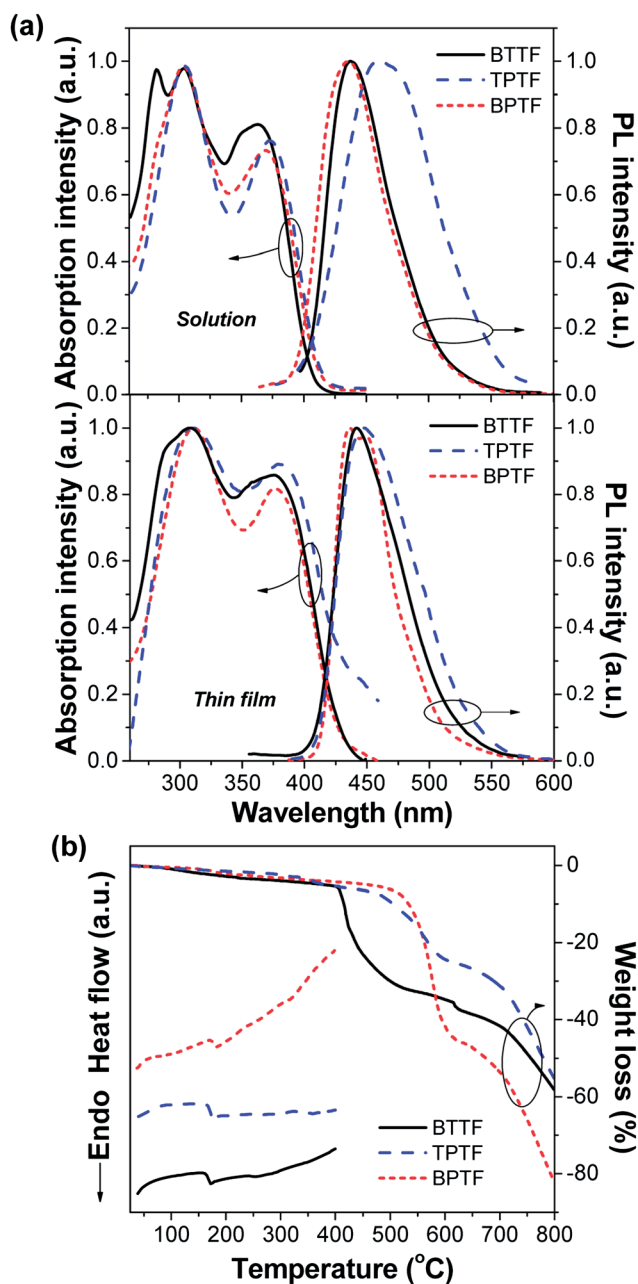


Fig. 3 (a) UV-vis absorption and PL spectra measured in CH_2Cl_2 solution and as thin film obtained by thermal deposition on a quartz substrate. (b) DSC (2nd heating scan) and TGA thermograms measured under N_2 at a heating rate of $10\text{ }^\circ\text{C min}^{-1}$.

morphological changes. The thermal properties of **BTTF**, **TPTF** and **BPTF** were investigated by the thermogravimetric analysis (TGA) and differential scanning calorimetry (DSC), and the results are shown in Fig. 3b and summarized in Table 1. Those results suggested that all compounds were thermally stable materials with 5% weight loss temperatures (T_{5d}) well over $390\text{ }^\circ\text{C}$. In the 1st and 2nd heating scans, DSC thermograms of all compounds displayed only a baseline shift due to glass transition temperatures (T_g) ranging from 171 to $179\text{ }^\circ\text{C}$ with no crystallization and melting peaks observed at higher temperatures. These results indicated that these materials were stable amorphous

materials with high T_g which was higher than those of the commonly used HTMs such as NPB ($T_g = 100\text{ }^\circ\text{C}$) and N,N' -bis(3-methylphenyl)- N,N' -bis(phenyl)benzidine (TPD) ($T_g = 63\text{ }^\circ\text{C}$), and other triphenylamine derivatives.²⁰ The results proved that the use of 9,9-bis(4-diphenylaminophenyl)fluorene as a molecular platform could reduce the crystallization of pyrene and improve the amorphous stability of the materials, which in turn could increase the service time in device operation and enhance the morphological stability of the thin film.²¹ Moreover, the abilities of these materials to form molecular glass and dissolve in organic solvents offer the possibility to prepare good thin films by both thermal evaporation and solution casting techniques which are highly desirable for fabrication of an OLED device.

Electrochemical behaviours of all compounds were investigated by cyclic voltammetry (CV), and the resulting data are shown in Fig. 4 and summarized in Table 1. The experiment was carried out in degassed CH_2Cl_2 containing $0.1\text{ M } n\text{-Bu}_4\text{NPF}_6$ as a supporting electrolyte under argon atmosphere. **BTTF** was found to exhibit one quasi-reversible oxidation process at 0.96 V , while both **TPTF** and **BPTF** showed two quasi-reversible oxidation processes with an additional peak at a lower potential (0.74 V) on the cathodic scan (E_{pc}) being observed. The first oxidation potentials of all compounds were nearly identical ($0.96\text{--}0.98\text{ V}$) and were assigned to the removal of electrons from the triphenylamines resulting in radical cations as demonstrated in Fig. 5. The multiple CV scans of **BTTF** revealed identical CV curves, indicating no oxidative coupling or a weak oxidative coupling if any at *p*-phenyl rings of the peripheral triphenylamine led to electro-polymerization and **BTTF** is electrochemically stable molecule. However, this type of electrochemical reaction was detected in both **TPTF** and **BPTF** as indicated by the presence of the cathodic peak at 0.74 V in their first CV scan. The repeated CV scans of these compounds also revealed an increasing change in their CV curves as illustrated in Fig. S1 (ESI[†]). Usually, this type of electrochemical coupling reaction is detected in most triphenylamine derivatives with unsubstituted *p*-position of the phenyl ring such as in the case of 2,7-bis-[2-(4-diphenylaminophenyl)-1,3,4-oxadiazol-5-yl]-9,9-bis-*n*-hexylfluorene.²² A proposed oxidation and electrochemical coupling reaction of these materials is outlined in Fig. 5. During the first oxidation, the electrons are removed from the *N*-atom of all available triphenylamine moieties to give a radical cation form **A** which undergoes electron delocalization to get resonance forms **B**, **C** and **D**, respectively. These radical cations are highly reactive

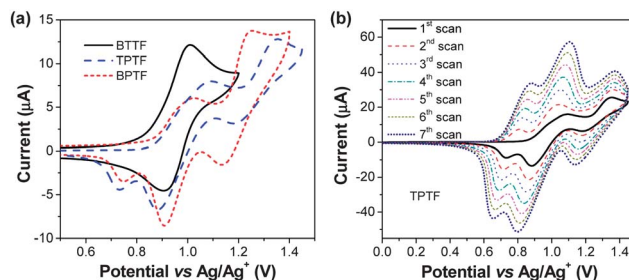


Fig. 4 (a) CV curves of **BTTF**, **TPTF** and **BPTF** and (b) multiple CV scans of **TPTF** measured in CH_2Cl_2 at a scan rate of 50 mV s^{-1} .

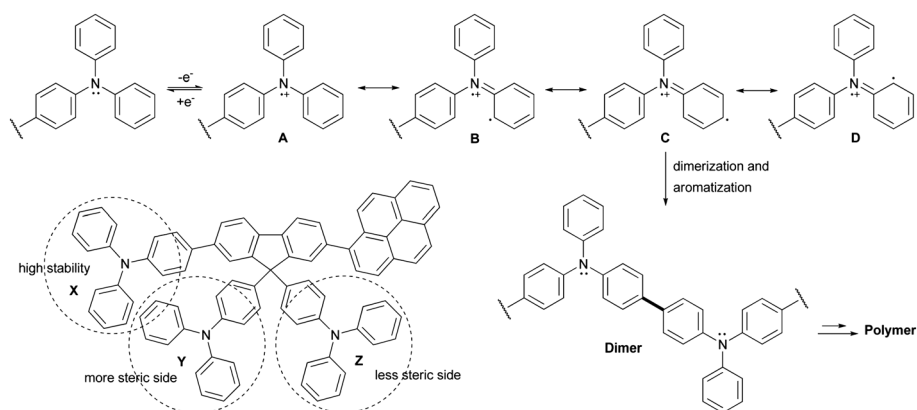


Fig. 5 A proposed oxidation and electrochemical reaction of the triphenylamine moiety.

species and readily undergo dimerization coupling to form a stable neutral molecule. Resonance forms **A**, **B** and **D** having a radical on the N atom and *ortho*-C atoms, respectively, are less reactive to a dimerization coupling reaction due to high steric hindrance and thereby this electrochemical reaction would take place through the resonance form **C**. However, triphenylamine units **X** and **Y** are unlikely to undergo such a coupling reaction because the radical cation formed is stabilized by electron delocalization through the attached fluorene ring^{20a} and is prevented by the steric hindrance of the adjacent triphenylamine unit, respectively. Hence, the oxidative coupling of the triphenylamine occurs only with the unstable and less steric triphenylamine unit **Z**. Steric hindrance and stability of triphenylamine moieties therefore played an important role in preventing such an electrochemical reaction in **BTTF**. While in cases of **TPTF** and **BPTF** having one or both of C-2 and -7 positions of the fluorene ring being substituted by a pyrene ring which is less bulky than the triphenylamine unit (in **BTTF**), the coupling reaction took place through less steric triphenylamine pendant groups (**X**). However, this type of electrochemical reaction will become inactive in the non-diffusion system or solid state. Moreover, under these CV experiment conditions, no distinct reduction process was observed in all cases. The HOMO and LUMO energy levels of **BTTF**, **TPTF** and **BPTF** were calculated from the oxidation onset potentials (E_{onset}) and energy gaps (E_g) and the results are summarized in Table 1. The HOMO levels of these

materials ranged from 5.29 to 5.31 eV matching well with the work functions of the gold (Au) or indium tin oxide (ITO) electrodes and hence favouring the injection and transport of holes.

Electroluminescent properties

Owing to their high blue fluorescence ($\Phi_F = 0.43\text{--}0.74$) and their HOMO levels (5.30 eV) lying between those of PEDOT:PSS (5.00 eV) and Alq3 (5.80 eV), the new synthesized materials **BTTF**, **TPTF** and **BPTF** could be used as bifunctional materials namely blue light-emitting and hole-transporting materials. This encouraged us to investigate the use of these compounds as an emissive layer (EML) for blue OLED and hole-transporting layer (HTL) for Alq3-based green OLED. The blue light-emitting diodes with the device structure of indium tin oxide (ITO)/PEDOT:PSS/EML(50 nm)/BCP(40 nm)/LiF(0.5 nm):Al(150 nm) and green light-emitting diodes with the device structure of ITO/PEDOT:PSS/HTL(40 nm)/Alq3(50 nm)/LiF(0.5 nm):Al(150 nm) were fabricated. Tris-(8-hydroxyquinoline) aluminium (Alq3) acts as the green light-emitting (EML) and electron-transporting layers (ETL). Conductive polymer, poly(3,4-ethylenedioxythiophene):poly(4-styrenesulfonate) (PEDOT:PSS), as the hole injection layer and 2,9-dimethyl-4,7-diphenyl-1,10-phenanthroline (BCP) as the hole blocking layer (HBL) were integrated to enable high-performance devices. From our study and

Table 2 Device characteristics of the fabricated OLED devices

Device	Structure	V_{on}^a	λ_{max}^b	L_{max}^c	η^d	EQE^e	CIE^f
I	ITO/PEDOT:PSS/ BTTF /BCP/LiF:Al	3.3	427	2340	0.83	0.22	0.16, 0.08
II	ITO/PEDOT:PSS/ TPTF /BCP/LiF:Al	3.3	437	3639	0.88	0.29	0.15, 0.12
III	ITO/PEDOT:PSS/ BPTF /BCP/LiF:Al	3.4	438	6245	2.06	0.56	0.15, 0.13
IV	ITO/PEDOT:PSS/NPB/BCP/LiF:Al	3.4	436	343	0.73	0.24	0.15, 0.07
V	ITO/PEDOT:PSS/ BTTF /Alq3/LiF:Al	3.1	519	28 895	4.78	0.23	0.29, 0.53
VI	ITO/PEDOT:PSS/ TPTF /Alq3/LiF:Al	3.2	518	26 375	4.88	0.24	0.28, 0.53
VII	ITO/PEDOT:PSS/ BPTF /Alq3/LiF:Al	3.0	519	30 760	4.94	0.24	0.29, 0.52
VIII	ITO/PEDOT:PSS/NPB/Alq3/LiF:Al	3.1	516	30 044	4.45	0.22	0.30, 0.54
IX	ITO/ BPTF /Alq3/LiF:Al	5.9	520	1236	1.24	0.06	0.27, 0.53
X	ITO/PEDOT:PSS/Alq3/LiF:Al	4.2	518	4961	0.91	0.05	0.30, 0.54

^a Turn-on voltage (V) at a luminance of 1 cd m⁻². ^b Emission maximum. ^c Maximum luminance (cd m⁻²) at the applied voltage (V). ^d Luminance efficiency (cd A⁻¹). ^e External quantum efficiency (%). ^f CIE coordinates (x, y).

other reports,²³ it was found that the incorporation of PEDOT:PSS in the device as the hole injection layer not only increased the maximum luminance from 1236 cd m^{-2} (η of 1.24 cd A^{-1}) in device IX to 30 760 cd m^{-2} (η of 4.94 cd A^{-1}) in device VII, but also significantly decreased the turn-on voltage from 5.9 V to 3.0 V (Table 2). Moreover, their EL spectra were near identical. It has been pointed out that the lower operating voltage of the PEDOT:PSS-based device can be attributed to the rough and porous surface of the spin-coated PEDOT:PSS polymer layer, which increases the contact area to enhance hole injection and lowers the barrier at the organic–organic interface by relocating the barrier to the more conductive PEDOT:PSS layer.²⁴ To enable high-performance devices therefore PEDOT:PSS as the hole injection layer was integrated into all devices. To compare the blue light-emitting and hole-transporting abilities of the synthesized materials, *N,N'*-diphenyl-*N,N'*-bis(1-naphthyl)-(1,1'-biphenyl)-4,4'-diamine (NPB), a commonly used commercial HTM, was employed as reference EML and HTL materials and the reference devices (IV and VIII) of the same structure were fabricated.

As non-doped blue emitters, under an applied voltage, devices I–III emitted a bright blue light with peaks centered at 427, 437 and 438 nm, respectively (Fig. 6a). The electroluminescence (EL) spectra of all diodes matched with their corresponding PL spectra with the EL of device I being slightly blue shifted (9 nm) from the PL of **BTTF**. Moreover, no emission shoulder at the longer wavelength owing to excimer and exciplex species formed at the interface of EML and HBL materials, which often occurs in the devices fabricated from EML with a planar molecular structure, was detected. In our case, the formation of these species could be prevented by the bulky nature of the 9,9-bis(4-diphenylaminophenyl)fluorene implemented as the molecular

platform. Additionally, a stable emission was obtained from all devices and the EL spectra did not change much over the entire drive voltages (Fig. S2, ESI†). Device I emitted a deep blue (427 nm) light with *CIE* coordinates of (0.16, 0.08), which is close to the National Television System Committee (NTSC) deep blue (0.14, 0.10) standard. The voltage–luminance and voltage–current density (*J–V–L*) characteristics of the devices are shown in Fig. 6b–d, and their electrical parameters are summarized in Table 2. The light turn-on voltage at 1 cd m^{-2} for all devices was in the range of 3.3–3.4 V and the operating voltage at 100 cd m^{-2} was in the range of 4.0–5.0 V, indicating good performance is achieved for all the devices. The device characteristics in terms of maximum brightness, turn-on voltage and maximum luminous efficiency clearly verified that the blue-emitting abilities of these newly synthesized materials were greater than the NPB-based device (device IV). The results also revealed that **BPTF** bearing two pyrene rings attached to the fluorene ring of the 9,9-bis(4-diphenylaminophenyl)fluorene had the best EML properties among these three materials. The device (III) showed a high maximum brightness of 6245 cd m^{-2} at 8.8 V, a low turn-on voltage of 3.4 V, a maximum luminous efficiency of 2.06 cd A^{-1} and a maximum external quantum efficiency of 0.56%. A reasonably lower device performance was observed in devices I (**BTTF** as EML) and II (**TPTF** as EML) displaying a maximum luminous efficiency of 0.83 and 0.88 cd A^{-1} , respectively. The trend in device luminous efficiencies matched very well with the observed decrease in PL quantum efficiencies in going from **BPTF** to **TPTF** to **BTTF** (Table 1). The fluorescence quantum yield (Φ_F) of **BPTF** was significantly higher than those of **TPTF** and **BTTF**. It has been demonstrated that the efficiency of an OLED depends both on the balance of electrons and holes and the Φ_F of the emitter.²⁵ Analysis of the band energy diagrams of

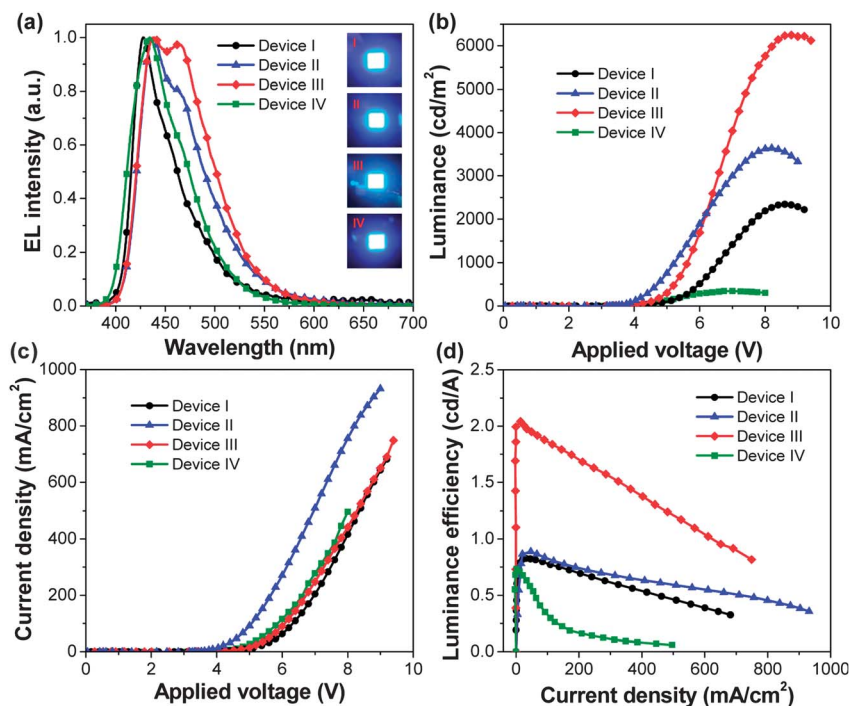


Fig. 6 (a) EL spectra, (b) *V–L* characteristics, (c) *I–V* characteristics, and (d) variation of luminance efficiency with current density of the fabricated blue OLED devices using the synthesized materials as EML.

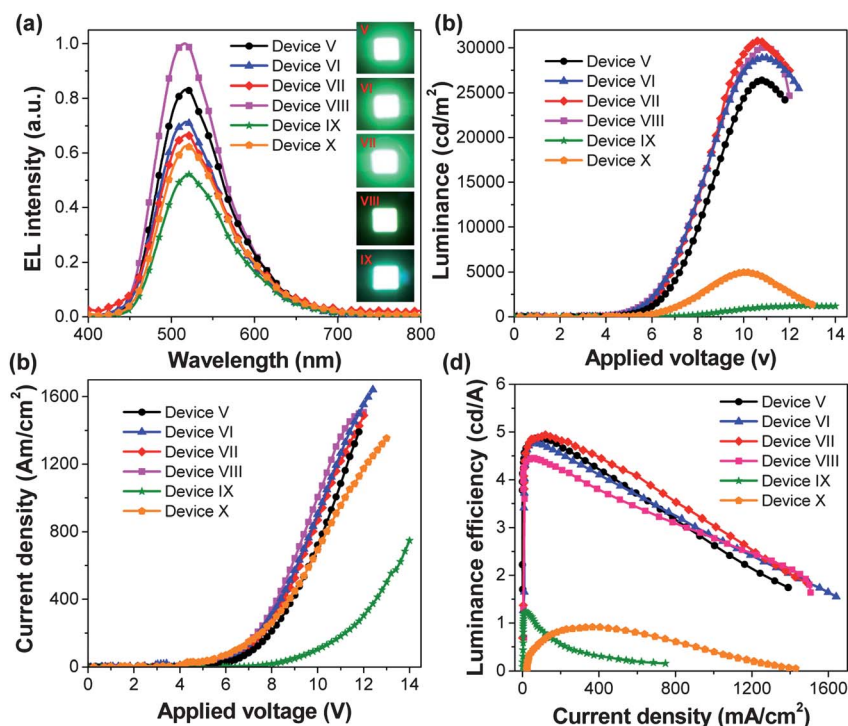


Fig. 7 (a) EL spectra, (b) V - L characteristics, (c) I - V characteristics, and (d) variation of luminance efficiency with current density of the fabricated green OLED devices using the synthesized materials as HTL.

these diodes also revealed that the HOMO levels of **BTTF**, **TPTF** and **BPTF** (5.28–5.31 eV) sat perfectly between those of the hole injection layer (PEDOT:PSS, 5.00 eV) and HBL (BCP, 6.50 eV), resulting in the charge efficiently recombining in the emitting layer and better device performance (Fig. S3, ESI†).

As HTLs, devices (V–VII) exhibited the light turn-on voltage at 1 cd m^{-2} in the range of 3.0–3.1 V and the operating voltage at 100 cd m^{-2} in the range of 4.2–4.6 V, indicating good performance is achieved for all the devices (Fig. 7 and Table 2). By comparison with the reference device X, it was found that the incorporation of **BTTF**, **TPTF** and **BPTF** in the device as HTL not only increased the maximum luminance from 4961 cd m^{-2} (η of 0.91 cd A^{-1}) to $26\,375$ – $30\,760 \text{ cd m}^{-2}$ (η of 4.78 – 4.94 cd A^{-1}) in device III, but also significantly decreased the turn-on voltage from 4.2 V to 3.0–3.2 V. Besides, their EL spectra were nearly identical. Moreover, the device characteristics in terms of luminous efficiency clearly demonstrated that the HTM abilities of these materials were greater than the NPB-based device (device VIII). Device VII having compound **BPTF** as HTL exhibited the best performance with a high maximum brightness of $30\,760 \text{ cd m}^{-2}$ for green OLED at 10.6 V, a low turn-on voltage of 3.0 V, a maximum luminous efficiency of 4.94 cd A^{-1} and a maximum external quantum efficiency of 0.24%. A comparable device performance was observed from devices V (**BTTF** as HTL) and VI (**TPTF** as HTL) (Table 1). Under an applied voltage, all devices (V–VII) exhibited a bright green emission with peaks centered at 519 nm and CIE coordinates of (0.29, 0.53) (Fig. 7a). The electroluminescence (EL) spectra of these diodes were identical, and matched with the PL spectrum of Alq3, the EL spectra of the reference devices (VII and X) and also other reported EL spectra of Alq3-based devices.²⁶ No emission at the

longer wavelength owing to exciplex species formed at the interface of HTL and ETL materials, which often occurs in the devices fabricated from HTL with a planar molecular structure, was detected.²⁷ In our case, the formation of exciplex species could be prevented by the bulky nature of the 9,9-bis(4-diphenylaminophenyl)fluorene. From device performance results and the fact that the barrier for electron-migration at the Alq3/HTL interface ($\sim 0.7 \text{ eV}$) is higher than that for hole-migration at the HTL/Alq3 interface ($\sim 0.5 \text{ eV}$), under the present device configuration of ITO/PEDOT:PSS/HTL(50 nm)/Alq3(50 nm)/LiF(0.5 nm):Al(200 nm), **BTTF**, **TPTF** and **BPTF** would act only as HTLs, and Alq3 would act preferably as an electron blocker more than as a hole blocker, and charge recombination was thus confined to the Alq3 layer. More importantly, a stable emission was obtained from all diodes (V–VII) and the EL spectra and CIE coordinates did not change over the entire applied voltages (Fig. S4, ESI†).

Although, many blue emitting and hole-transporting materials have been reported, in terms of the amorphous morphology, high T_g and device efficiency, **BPTF** is among the good bifunctional materials reported.

Conclusions

In conclusion, we successfully designed and synthesized three bifunctional materials namely **BTTF**, **TPTF** and **BPTF**. By the use of 9,9-bis(4-diphenylaminophenyl)fluorene as a molecular platform, we were able to reduce the crystallization and maintained high blue emissive ability of pyrene in the solid state, and improved the amorphous stability of these materials. Strong blue emission in both solution and solid state with solution

fluorescence quantum efficiency up to 74% was obtained. All of them were thermally stable amorphous materials with a glass transition temperature well above 170 °C. Their abilities as both blue light-emitting materials for blue OLEDs and hole-transporting materials for green OLEDs in terms of device performance and thermal property were greater than a commonly used NPB. Importantly, **BPTF** having two pyrene rings as terminal substituents showed promising potential as both blue light-emitting and hole-transporting materials for OLED devices. Non-doped blue OLEDs with a maximum luminance efficiency of 2.06 cd A⁻¹, and green OLEDs with a maximum luminance efficiency of 4.94 cd A⁻¹ were obtained. The use of this type of molecular platform might be an effective way to prepare high T_g amorphous materials for long-lifetime device applications, especially for high-temperature applications in OLEDs or other organic optoelectronic devices.

Acknowledgements

This work was financially supported by the Thailand Research Fund (RMU5080052). We acknowledge the scholarship support from Center of Excellence for Innovation in Chemistry (PERCH-CIC), Ubon Ratchathani University, and the Office of the Higher Education Commission, Thailand.

Notes and references

- 1 B. W. D'Andrade and S. R. Forrest, *Adv. Mater.*, 2004, **16**, 1585.
- 2 (a) A. Thangthong, D. Meunmart, T. Sudyoadsuk, S. Jungstittiwong, N. Prachumrak, T. Keawin and V. Promarak, *Chem. Commun.*, 2011, **47**, 7122; (b) E. Wang, C. Li, Y. Mo, Y. Zhang, G. Ma, W. Shi, J. Peng, W. Yang and Y. Cao, *J. Mater. Chem.*, 2006, **16**, 4133; (c) S.-H. Liao, J.-R. Shiu, S.-W. Liu, S.-J. Yeh, Y.-H. Chen, C.-T. Chen, T. J. Chow and C.-I. Wu, *J. Am. Chem. Soc.*, 2009, **131**, 763.
- 3 G. Grem, G. Leditzky, B. Ullrich and G. Leising, *Adv. Mater.*, 1992, **4**, 36.
- 4 (a) S. Kappaun, H. Scheiber, R. Trattnig, E. Zojer, E. J. W. List and C. Slugovc, *Chem. Commun.*, 2008, 5170; (b) J. Huber, K. Müllen, J. Salbeck, H. Schenk, U. Scherf, T. Stehlin and R. Stern, *Acta Polym.*, 1994, **45**, 244; (c) M. R. Craig, M. M. de Kok, J. W. Hofstra, A. P. H. J. Schenning and E. W. Meijer, *J. Mater. Chem.*, 2003, **13**, 2861.
- 5 D. Vak, C. Chun, C. L. Lee, J.-J. Kim and D.-Y. Kim, *J. Mater. Chem.*, 2004, **14**, 1342.
- 6 (a) S. Setayesh, A. C. Grimsdale, T. Weil, V. Enkelmann, K. Müllen, F. Meghdadi, E. J. W. List and G. Leising, *J. Am. Chem. Soc.*, 2001, **123**, 946; (b) E. J. W. List, R. Guentner, P. Scandiucci de Freitas and U. Scherf, *Adv. Mater.*, 2002, **14**, 374; (c) J.-I. Lee, V. Y. Lee and R. D. Miller, *ETRI J.*, 2002, **24**, 409.
- 7 D. Sainova, T. Miteva, H. G. Nothofer, U. Scherf, I. Glowacki, J. Ulanowski, H. Fujikawa and D. Neher, *Appl. Phys. Lett.*, 2000, **76**, 1810.
- 8 T. Miteva, A. Meisel, W. Knoll, H. G. Nothofer, U. Scherf, D. C. Müller, K. Meerholz, A. Yasuda and D. Neher, *Adv. Mater.*, 2001, **13**, 565.
- 9 (a) C.-S. Wu and Y. Chen, *J. Mater. Chem.*, 2010, **20**, 7700; (b) J.-I. Lee, H. Y. Chu, H. Lee, J. Oh, L.-M. Do, T. Zyung, J. Lee and H.-K. Shim, *ETRI J.*, 2005, **27**, 181.
- 10 C. Ego, A. C. Grimsdale, F. Uckert, G. Yu, G. Srdanov and K. Müllen, *Adv. Mater.*, 2002, **14**, 809.
- 11 M. Surin, E. Hennebicq, C. Ego, D. Marsitzky, A. C. Grimsdale, K. Müllen, J.-L. Brédas, R. Lazzaroni and P. Leclère, *Chem. Mater.*, 2004, **16**, 994.
- 12 (a) T. Zhang, D. Liu, Q. Wang, R. Wang, H. Ren and J. Li, *J. Mater. Chem.*, 2011, **21**, 12969; (b) L. S. Chinelatto, Jr, J. del Barrio, M. Piñol, L. Oriol, M. A. Matranga, M. P. De Santo and R. Barberi, *J. Photochem. Photobiol., A*, 2010, **210**, 130; (c) V. Promarak, S. Saengsuwan, S. Jungstittiwong, T. Sudyoadsuk and T. Keawin, *Tetrahedron Lett.*, 2007, **48**, 89.
- 13 Z. Zhao, S. Chen, J. W. Y. Lam, Z. Wang, P. Lu, F. Mahtab, H. H. Y. Sung, I. D. Williams, Y. Ma, H. S. Kwok and B. Z. Tang, *J. Mater. Chem.*, 2011, **21**, 7210.
- 14 K. Fujimoto, S. Yamada and M. Inouye, *Chem. Commun.*, 2009, 7164.
- 15 C. Tang, F. Liu, Y.-J. Xia, L.-H. Xie, A. Wei, S.-B. Li, Q.-L. Fan and W. Huang, *J. Mater. Chem.*, 2006, **16**, 4074.
- 16 T. Kumchoo, V. Promarak, T. Sudyoadsuk, M. Sukwattanasinitt and P. Rashatasakhon, *Chem.-Asian J.*, 2010, **5**, 2162.
- 17 T. Kartens and K. Kobs, *J. Phys. Chem.*, 1980, **84**, 1871.
- 18 M. J. Frisch, G. W. Trucks, H. B. Schlegel, G. E. Scuseria, M. A. Robb, J. R. Cheeseman, V. G. Zakrzewski, J. A. Montgomery, Jr, R. E. Stratmann, J. C. Burant, S. Dapprich, J. M. Millam, A. D. Daniels, K. N. Kudin, M. C. Strain, O. Farkas, J. Tomasi, V. Barone, M. Cossi, R. Cammi, B. Mennucci, C. Pomelli, C. Adamo, S. Clifford, J. Ochterski, G. A. Petersson, P. Y. Ayala, Q. Cui, K. Morokuma, D. K. Malick, A. D. Rabuck, K. Raghavachari, J. B. Foresman, J. Cioslowski, J. V. Ortiz, B. B. Stefanov, G. Liu, A. Liashenko, P. Piskorz, I. Komaromi, R. Gomperts, R. L. Martin, D. J. Fox, T. Keith, M. A. Al-Laham, C. Y. Peng, A. Nanayakkara, C. Gonzalez, M. Challacombe, P. M. W. Gill, B. G. Johnson, W. Chen, M. W. Wong, J. L. Andres, M. Head-Gordon, E. S. Replogle and J. A. Pople, *Gaussian 98, Revision A.7*, Gaussian, Inc., Pittsburgh, PA, 1998.
- 19 S. R. Forrest, D. D. C. Bradley and M. E. Thomson, *Adv. Mater.*, 2003, **15**, 1043.
- 20 (a) V. Promarak, M. Ichikawa, T. Sudyoadsuk, S. Saengsuwan and T. Keawin, *Opt. Mater.*, 2007, **30**, 364; (b) D. Seka, E. Grabcica, H. Janeczeka, B. Jarzabeka, B. Kaczmarczyka, M. Domanska and A. Iwan, *Opt. Mater.*, 2010, **32**, 1514.
- 21 R. Fink, Y. Heischkel, M. Thelakkat and H. Schmidt, *Chem. Mater.*, 1998, **10**, 3620.
- 22 K. T. Kamtekar, C. Wang, S. Bettington, A. S. Batsanov, I. F. Perepichka, M. R. Bryce, J. H. Ahn, M. Rabinal and M. C. Petty, *J. Mater. Chem.*, 2006, **16**, 3823.
- 23 S. Kirchmeyer and K. Reuter, *J. Mater. Chem.*, 2005, **15**, 2077.
- 24 W. Kim, G. Kushto, G. Kim and Z. Kafafi, *J. Polym. Sci., Part B: Polym. Phys.*, 2003, **41**, 2522.
- 25 U. Mitschke and P. BaÈuerle, *J. Mater. Chem.*, 2000, **10**, 1471.
- 26 (a) A. Thaengthong, S. Saengsuwan, S. Jungstittiwong, T. Keawin, T. Sudyoadsuk and V. Promarak, *Tetrahedron Lett.*, 2011, **52**, 4749; (b) Y. K. Kim and S.-H. Hwang, *Synth. Met.*, 2006, **156**, 1028.
- 27 D. Y. Kim, H. N. Cho and C. Y. Kim, *Prog. Polym. Sci.*, 2000, **25**, 1089.